Outlet Diameter and the Vortex Generated by an Air Cannon

Smith Thamakaison*,[1] Zihao Ye[1], Orakanya Junthaha[2], Aunyawee Piriyachatchai[2],

1. *International School Bangkok, 39/7 Samakee Road, Pakkret, Nonthaburi, Thailand 11120*
2. *Kamnoetvidya Science Academy, 999 Moo 1 Payupnai, Wangchan, Rayong 21210*

**Email: mattthamakaison@gmail.com*

Abstract

Air vortex cannons generate structurally integral, coherent rings of rotating air that propagate through a surrounding medium over measurable distances. The effect of the outlet diameter of an air vortex cannon on the mass, impulse, and average velocity of air vortices produced by the cannon was investigated experimentally. Vortices generated using six outlet diameters were analysed by measuring the impulse exerted on a force plate and the impact velocity, from which the effective vortex mass was calculated. Increasing outlet diameter resulted in a monotonic power-law increase in both vortex mass and impulse, while the average velocity reached a maximum at an intermediate outlet diameter before decreasing. These results indicate that vortex performance depends on balancing the volume of air expelled with the ability to maintain vortex coherence, suggesting the existence of an optimal outlet diameter for effective vortex formation.

***Keywords*:** Air vortex, Vortex rings, Outlet diameter, Impulse, Airflow dynamics, Fluid mechanics

I. INTRODUCTION

During the later years of the Second World War, Germany pursued a wide range of experimental weapons to gain strategic advantage over the enemy. Among these was an unconventional anti-aircraft concept known as the Windkanone ("wind cannon"), which used large, impulsive bursts of air in the form of structurally uniform vortex rings in order to disturb or destroy enemy aircraft. The concept was designed for the device to expel a concentrated puff of air through a circular outlet, forming an air vortex that would travel forward with a sufficient velocity and momentum to affect aircraft stability. Despite a significant engineering and architectural effort, the Windkanone ultimately failed due to the fact that the generated vortices rapidly dissipated and lacked the impulse and structural integrity required at operational distances.

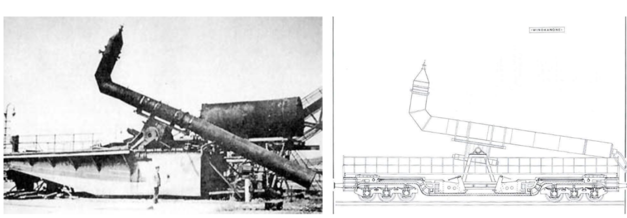

Figure 1. The 'Windkanone' German Technological Weapon.[1]

Although unsuccessful as a weapon, the Windkanone represents an early engineered attempt to exploit the physics of air vortex rings. Air vortex rings have been studied since the end of the nineteenth century, with Sir William Thomson providing fundamental explanations for their formation mechanisms.[2] A vortex ring (or "toroidal" vortex) is a torus-shaped vortex (Figure 2) in a finite volume of fluid. It is typically created when fluid is impulsively expelled through an orifice, where the dominant flow is characterized by fluid spinning around an imaginary axis line that forms a closed loop.[3] These structures demonstrate remarkable stability and can travel considerable distances while maintaining their shape.

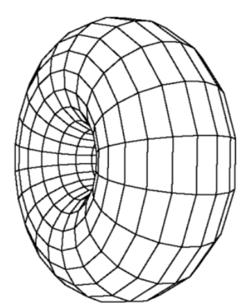

Figure 2. Illustration of a toroid.

Previous research conducted by McKeag utilized comprehensive experiments analyzing air vortex rings traveling through air over distances of four meters.[4] Using Logger Pro software for video analysis, velocity measurements as functions of distance were obtained, along with impulse measurements using force plates at various distances. These data were combined to determine vortex mass variations with distance traveled. McKeag's findings revealed that vortex mass reaches a minimum at approximately two meters, potentially resulting from the shedding of initial non-spinning air mass under friction forces from surrounding air. Following McKeag's work, Liang[5] conducted a more precise investigation that addressed methodological limitations in the original study. The key findings from Liang's research extended McKeag's observations regarding minimum mass at two meters. Liang demonstrated that once the vortex fully formed at 2.0 meters, there was an approximately linear increase in vortex mass with distance, up to 4.5 meters. This increase was attributed to the vortex enlarging by winding in still air as it traveled. The measured vortex masses ranged from 5 to 10 grams, corresponding to vortex volumes of approximately 4000 to 8000 cc, based on air density of 1.20 kg per cubic meter at 20°C.

This investigation extends the work of McKeag and Liang by examining how outlet geometry influences key physical properties of vortex rings. Specifically, this study investigates the relationship between relative outlet diameter (defined as outlet diameter divided by the internal diameter of the cannon) and three quantities: average velocity, impulse, and mass of the vortex ring measured at a distance of 4.0 m from the cannon.

Following McKeag and Liang, impulse is determined from force-time measurements using:

$$J = \int F(t)\, dt \qquad (1)$$

and is equivalent to the momentum of the vortex at the measurement location:

$$J = mv \qquad (2)$$

where J is the momentum of the air vortex, m is its mass, and v is its average velocity. This relationship forms the basis for evaluating how outlet diameter affects the momentum of the generated vortex ring.

If the outlet diameter is too small, viscous losses and flow separation suppress vortex roll-up, preventing coherent ring formation.[6] Conversely, if the outlet diameter is too large, the shear layer becomes too weak to generate strong circulation, resulting in a diffuse and unstable vortex.[7] Therefore, an intermediate relative outlet diameter is predicted to optimize vortex formation by balancing airflow volume and rotational coherence.

II. METHODS

The experimental apparatus consisted of a cylindrical plastic container with a length of 60 cm, a rear diameter of 44 cm, and a circular outlet diameter of 33 cm. The outlet was covered by a heavy plastic sheet secured with elastic bands to form a flexible diaphragm. Two identical elastic bands were stretched from the front of the cannon to the rear of the outlet to create the propulsion mechanism. The rubber bands had a relaxed length of 15 cm and could be stretched to a maximum displacement of 16 cm during operation. The cannon was secured on a table to provide a stable base throughout all experimental trials (Figure 3).

The air cannon was aimed toward the center of a custom-built force plate composed of four Vernier dual-range force sensors arranged in a 2 × 2 orthogonal array and mounted at the corners of a rigid plastic board measuring 1 m × 1 m (Figure 4).

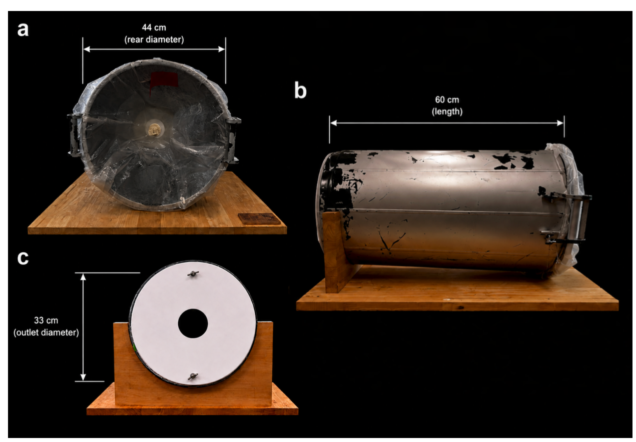

Figure 3. The air cannon used in all trials. (a) Rear view showing the breech end with the diaphragm release handle at the center. (b) Side view showing the cannon in its horizontal mounting position. (c) Front view showing the muzzle end with the central opening.

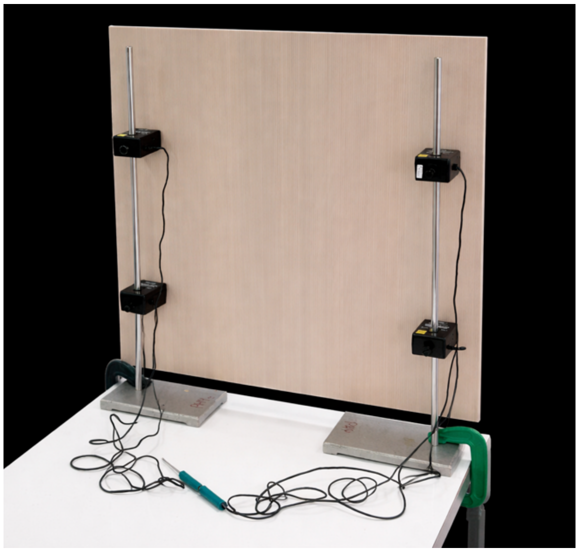

Figure 4. Plastic board used with four dual-range force probes fixed to the board and attached to clamp stands.

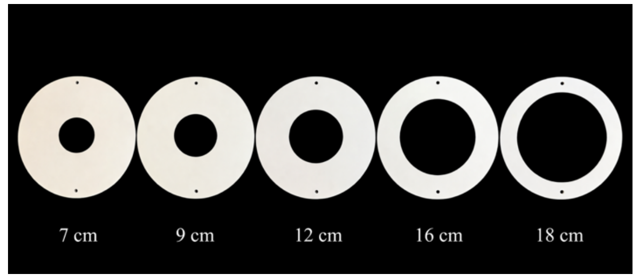

Figure 5. Interchangeable plastic covers used with relative outlet diameters ranging from 7 to 18 cm.

Five interchangeable outlet covers with diameters ranging from 7.0 cm to 18.0 cm (Figure 5) were tested. These were also expressed as relative outlet diameters (outlet diameter divided by cannon diameter). The force plate was positioned 4.0 m from the air cannon.

To visualize the behavior of the vortices, two smoke tablets were ignited and placed in a beaker. The beaker was placed inside the air cannon, and the outlet of the cannon was sealed with a lid for 45 seconds to allow smoke to accumulate. The lid was closed between trials to retain residual smoke and prevent premature release into the environment. This ensured consistent smoke density and vortex visibility across all four firings for each outlet diameter. To enhance video visibility, a large black backdrop was used. A 240 fps smartphone camera was positioned perpendicular to the vortex path. The full experimental area, including the cannon, force plate, and black backdrop, was captured in frame. For each outlet diameter, four vortex pulses were fired in succession, each separated by a 10-second interval to allow residual air and smoke to clear. This process was repeated for each of the five outlet diameters.

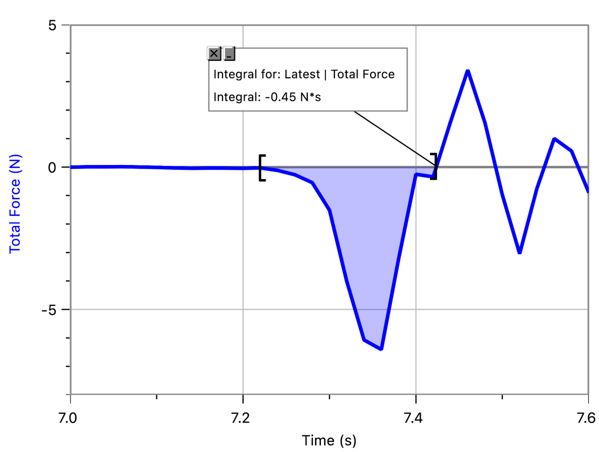

Figure 6. Representative force-time graph showing the summed force from all four sensors. The area under the curve (-0.45Ns) was taken as the impulse of the vortex.

The total force exerted by the vortex on the force plate was determined by summing the readings from all four force sensors during the impact of the vortex with the force plate, recording data at a rate of 100 samples per second. The impulse of each vortex was then calculated as the integral of the resulting force-time curve, as shown in figure 6.

To determine vortex velocity, the motion of the smoke ring was first tracked from the high-speed video. Figure 7 shows successive positions of the vortex marked at equal time intervals as it travelled toward the force plate. These tracked positions were then analyzed using the Logger Pro software to generate a position-time graph. A linear fit was applied to the position-time data obtained from the tracked vortex positions. The slope of the best-fit line, shown in figure 8, was taken as the average vortex velocity at a distance of 4.0 m from the cannon.

The effective mass of the vortex at impact was determined from the impulse and the velocity using Equation 2, assuming that the airflow was redirected parallel to the force plate after impact, resulting in a velocity component normal to the plate of zero.

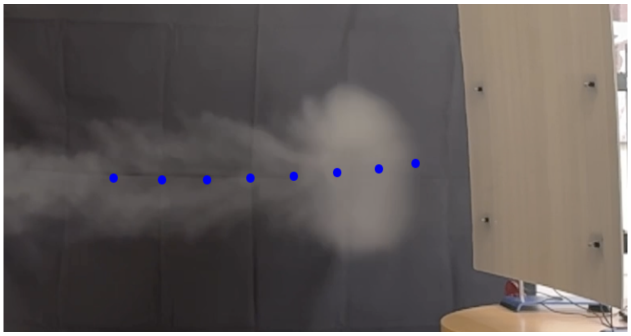

Figure 7. Representative successive positions of the vortex core during propagation. Blue markers indicate the vortex's tracked location at equal time intervals.

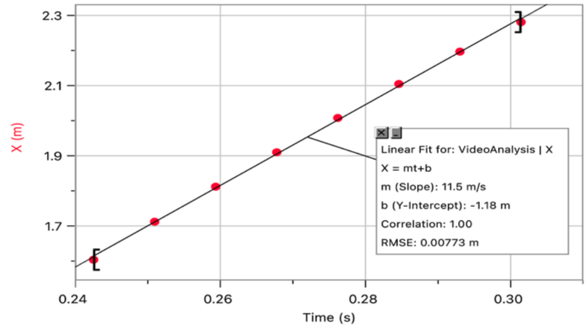

Figure 8. Representative position-time graph of the tracked vortex core. The slope of the linear fit represents the average vortex velocity.

III. RESULTS AND DISCUSSION

The results show that relative outlet diameter is a critical parameter influencing vortex behaviour, with distinct trends observed for each measured quantity. Figure 9 provides qualitative evidence of how outlet diameter influences vortex formation and propagation. Among the outlet diameters tested, the 16 cm outlet produced one of the most clearly defined vortex rings. The vortex remained visible over the greatest distance, maintained a relatively consistent size during propagation, and exhibited the vortex shedding behaviour described by Liang. The 12 cm outlet displayed similar characteristics, but with slightly greater spreading and dissipation as the vortex travelled away from the cannon.

		Distance from the cannon (cm)					
Hole diameter (cm)	**Relative Diameter**	**90**	**100**	**130**	**180**	**210**	**230**
		Time the vortex reaches the indicated distance (s)					
18	**0.55**	0.079 	0.092 	0.121 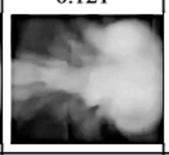	0.171 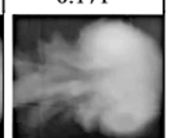	0.201 	0.226 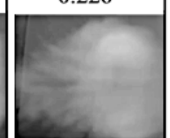
16	**0.49**	0.075 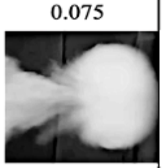	0.084 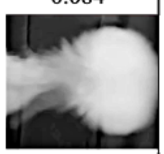	0.109 	0.151 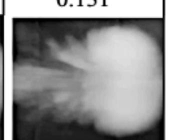	0.176 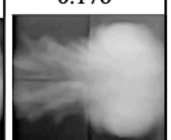	0.193 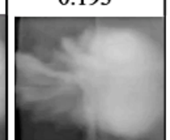
12	**0.36**	0.079 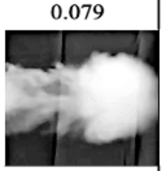	0.083 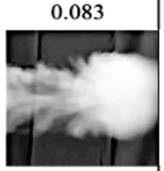	0.104 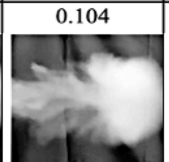	0.142 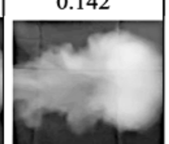	0.167 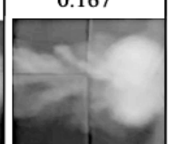	0.183 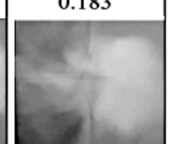
9	**0.27**	0.046 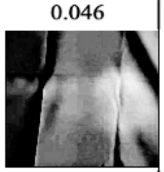	0.050 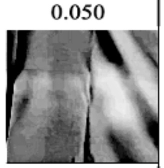	0.075 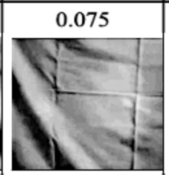	0.133 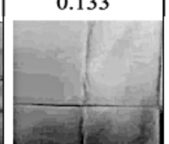	0.179 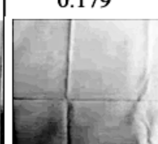	0.191 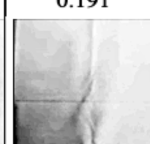
7	**0.21**	0.050 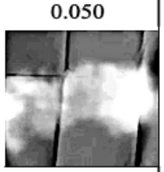	0.063 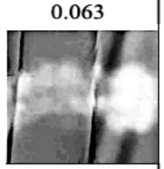	0.100 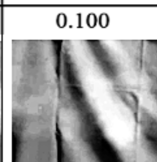	0.209 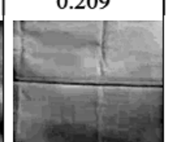	0.288 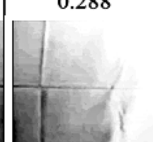	0.421 

Figure 9. Smoke visualization of vortex ring propagation for different outlet diameters at increasing distances from the cannon.

The 18 cm outlet also produced a well-defined vortex ring; however, the ring was noticeably larger and less uniform than those produced by the 12 cm and 16 cm outlets. As the vortex propagated, the smoke pattern spread and distorted further. Despite this, the vortex remained visible over a substantial distance and entrained a noticeably larger volume of smoke than the smaller outlet diameters.

In contrast, the 7 cm and 9 cm outlets produced only weak puffs of smoke, and a clearly defined vortex ring was rarely observed. The smoke dispersed rapidly and became indistinguishable from the surrounding air after a relatively short distance. Compared with the larger outlet diameters, these outlet sizes appeared unable to consistently generate a coherent vortex structure.

These qualitative observations are supported by the quantitatively recorded data discussed below from figures 10-12. The 12 cm and 16 cm nozzle sizes gave the greatest velocities whereas the 18 cm outlet provided the greatest impulse and effective mass. On the other hand, the faint and quick dissipating smoke structures seen in the 7 cm and 9 cm outlet sizes are unsurprising since they show relatively low velocities, impulses, and masses 4.0 m away from the cannon.

Figure 10 shows the relationship between vortex velocity and relative outlet diameter. Velocity increases with outlet diameter up to a maximum relative diameter of approximately 0.4, above which it decreases. This suggests the existence of an optimal outlet diameter for maximizing vortex speed. At small outlet diameters, airflow restriction and viscous losses limit vortex development and often prevent the formation of a coherent vortex ring. At larger outlet diameters, although a greater volume of air is expelled, the resulting vortex becomes broader and travels more slowly. This suggests that there is a trade-off between entraining a large volume of air and generating a fast-moving vortex that maintains its structural integrity over distance.

The relationship between outlet diameter and the mass of the air puff is shown in Figure 11. The data exhibit a strong non-linear increase in mass as outlet diameter increases. At smaller outlet diameters, the measured mass remains relatively low and varies only slightly within experimental uncertainty. However, beyond approximately 0.14 m, the mass increases rapidly. The data are well described by the empirical equation:

$$m = (4.4 \times 10^6)D^{11} + 0.013\ . \qquad (4)$$

Although this relationship lacks a theoretical basis, it provides a useful predictive model within the measured range and demonstrates the strong sensitivity of the entrained air mass to outlet diameter. The increased scatter alongside uncertainty at the smallest outlet diameter indicates inconsistent vortex formation, suggesting that excessive flow restriction limits the amount of air that can be coherently entrained into the vortex.

Figure 12 shows how impulse on impact at four meters distance from the cannon varies with outlet diameter. A clear increasing trend is observed across the entire range of diameters tested, with impulse rising sharply for larger outlet diameters. The data are well represented by the empirical relationship:

$$J = 1.6{D_R}^{2.1} \qquad (5)$$

At a distance of 4.0 m from the cannon, the relationship indicates that larger relative outlet

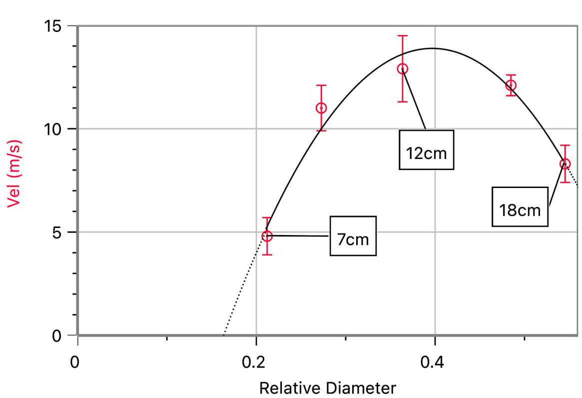

Figure 10. Relationship between velocity (v) and the hole diameter of the air cannon (D).

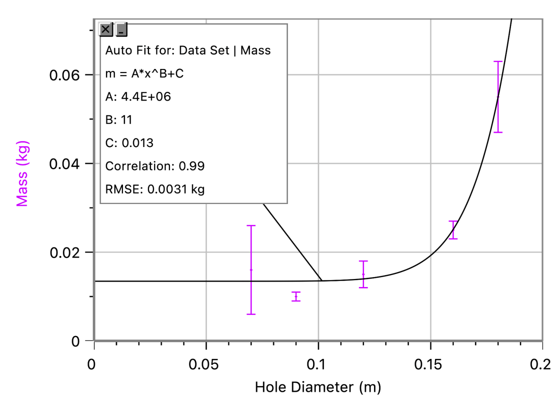

Figure 11. Relationship between mass (m) and the hole diameter of the air cannon (D).

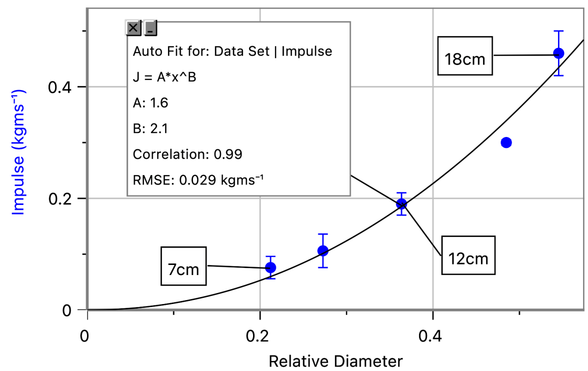

Figure 12. Relationship between the impulse (J) of the air vortex measured 4.0 m from the cannon and relative outlet diameter (D_R).

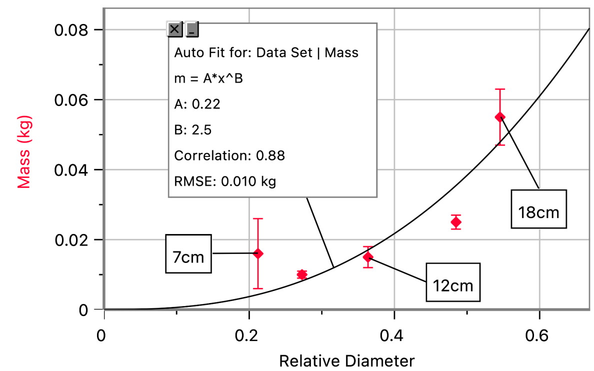

Figure 13. Relationship between the effective mass (m) of the air vortex measured 4.0 m from the cannon and the relative outlet diameter(D_R).

diameters generally produce vortices with greater measured impulse. However, the increase was not uniform. The 7 cm and 9 cm outlet diameters produced impulses close to zero, consistent with the smoke visualizations (Figure 9), in which the vortex rings were barely visible and did not develop into coherent structures capable of propagating over 4 m. In contrast, the 12 cm and 16 cm outlet diameters formed distinct, coherent vortex rings that maintained their structure over the propagation distance, resulting in a sharp increase in measured impulse. Although the 18 cm outlet diameter produced a less clearly defined vortex ring than the 12 cm and 16 cm diameters, the smoke visualizations showed that it generated a substantially larger air puff. This larger vortex size likely increased the momentum transferred to the force plate, explaining the further increase in measured impulse despite the reduced coherence of the vortex.

The relationship between outlet diameter and the mass of the air puff is shown in Figure 13. The data exhibit a positive relationship: an increase in mass corresponds to an increase in the outlet diameter. At smaller outlet diameters, the measured mass remains relatively low and varies only slightly within experimental uncertainty. The data can be described by the empirical power fit:

$$m = 0.22{D_R}^{2.5} \tag{6}$$

Although this relationship lacks a theoretical basis, it provides a useful predictive model within the measured range and demonstrates the strong sensitivity of the entrained air mass to outlet diameter. The increased scatter alongside uncertainty at the smallest outlet diameter indicates inconsistent vortex formation, suggesting that excessive flow restriction limits the amount of air that can be coherently entrained into the vortex.

The effective vortex masses measured in this investigation ranged from approximately 0.010 kg to 0.060 kg, which is larger than the 0.005–0.010 kg range reported by Liang for vortices measured between 2.0 m and 4.5 m from the cannon. This difference may be attributed to the larger cannon dimensions and outlet diameters used in the present investigation.

Overall, the results indicate that increasing the outlet diameter increases both the mass and impulse of the air puff, but does not necessarily increase the vortex velocity. Instead, the vortex's effectiveness depends on a balance between the volume of airflow and its coherence. The presence of a clear maximum in velocity indicates that an optimal outlet diameter exists that best satisfies this balance. These findings demonstrate that changing outlet diameter significantly affects vortex properties, and that an intermediate outlet diameter produces the most effective vortex under the conditions of this investigation.

IV. CONCLUSION

The effective mass of the vortex increased with outlet diameter following a power-law relationship, while the vortex velocity reached a maximum at an intermediate relative outlet diameter of around 0.4 before decreasing at larger diameters. Consequently, the impulse also increased with outlet diameter. These conclusions were supported by the smoke visualization, which showed that intermediate relative outlet diameters produced the most coherent and well-defined vortex rings over the greatest propagation distances, whereas the smallest diameters generated weak or poorly visible vortices and the largest diameters formed broader vortices that dispersed more rapidly. Therefore, it can be concluded that increasing outlet diameter alone does not necessarily improve vortex performance, and that an intermediate relative outlet diameter produces the most effective air vortex under the conditions of this investigation.

REFERENCES

1. *Wind cannon*. (n.d.). Nevington War Museum. Retrieved July 18, 2026, from https://www.nevingtonwarmuseum.com/wind-cannon.html

2. Thomson, W. (1869). 4. On vortex atoms [Review of *4. On vortex atoms*]. *Proceedings of the Royal Society of Edinburgh*, *6*, 94–105. https://doi.org/10.1017/s0370164600045430

3. Pulvirenti, F., Scollo, S., Ferlito, C., & Schwandner, F. M. (2023). Dynamics of volcanic vortex rings. *Scientific Reports*, *13*(1). https://doi.org/10.1038/s41598-022-26435-0

4. McKeag, P. (2006). *Vortex mass as a function of distance traveled*. Isb.Ac.Th. https://www2.isb.ac.th/physics_isb/physisb/students/iblabs/vortex2/vortex2.htm

5. Liang, S.-Y. (2007). Mass of an air cannon vortex. In *International Scholastic Journal of Science* (pp. 1–8). ISB Journal of Physics. https://www.isjos.org/pdfs/ISJOS_v1_p3.pdf

6. Kaplanski, F. B., & Rudi, Y. (2005). A model for the formation of ``optimal'' vortex rings taking into account viscosity. *Physics of Fluids*, *17*. https://www.researchgate.net/publication/252615646_a_model_for_the_formation_of_optimal

7. Limbourg, R., & Nedić, J. (2021). Formation of an orifice-generated vortex ring. *Journal of Fluid Mechanics*, *913*. doi.org/10.1017/jfm.2021.36